Extended Depth of Field Catadioptric Imaging Using Focal Sweep

Ryunosuke Yokoya*
Columbia University
New York, NY 10027
yokoya@cs.columbia.edu

Shree K. Nayar
Columbia University
New York, NY 10027
nayar@cs.columbia.edu

Abstract

Catadioptric imaging systems use curved mirrors to capture wide fields of view. However, due to the curvature of the mirror, these systems tend to have very limited depth of field (DOF), with the point spread function (PSF) varying dramatically over the field of view and as a function of scene depth. In recent years, focal sweep has been used extensively to extend the DOF of conventional imaging systems. It has been shown that focal sweep produces an integrated point spread function (IPSF) that is nearly space-invariant and depth-invariant, enabling the recovery of an extended depth of field (EDOF) image by deconvolving the captured focal sweep image with a single IPSF. In this paper, we use focal sweep to extend the DOF of a catadioptric imaging system. We show that while the IPSF is spatially varying when a curved mirror is used, it remains quasi depth-invariant over the wide field of view of the imaging system. We have developed a focal sweep system where mirrors of different shapes can be used to capture wide field of view EDOF images. In particular, we show experimental results using spherical and paraboloidal mirrors.

1. Introduction

Capturing images with wide fields of view is highly beneficial in applications such as surveillance, teleconferencing, and autonomous navigation [21, 22, 23, 28, 29]. Fisheye lenses and anamorphic lenses are often used to capture a wide field of view (FOV). However, they require the use of a large number of lenses to correct for various optical aberrations, and are difficult to design when the FOV is greater than a hemisphere. In contrast, catadioptric imaging systems, which use a combination of mirrors and lenses, provide the designer with significantly greater flexibility in terms of resolution and FOV [21, 22, 23, 28]. Since the optical properties of mirrors are independent of the wavelength of light, they do not produce chromatic aberrations like lenses do, which is a major advantage. However, when a curved mirror is used, the optical system suffers from greater field curvature and astigmatism which, in turn, severely limits the depth of field (DOF).

An image formed via a curved mirror, such as a spherical or a paraboloidal mirror, has spatially varying blur [1], which means that the entire FOV cannot be captured in focus with a single image. This problem is aggravated in low-light conditions, where the system needs to be operated with a low F-number (large aperture). The problem becomes even more prominent when the system uses an image sensor with a high resolution. One way to reduce the image blur caused by a curved mirror is to use additional (corrective) lenses, or multiple mirrors that offset each other's field curvature effects [25]. This, however, causes the system to be bulky and expensive.

A well-studied approach to extending the DOF of a conventional imaging system is focal sweep [2, 18, 20], in which the focal plane is translated during the exposure time of the image. It has been shown that a point spread function (PSF) of the captured image is both nearly space-invariant and nearly depth-invariant [20]. This PSF is called the integrated PSF (IPSF) and is used to deconvolve the captured image to obtain one that has large DOF, without a significant reduction in signal-to-noise ratio (SNR).

The goal of this paper is to explore the use of focal sweep to extend the DOF of a catadioptric imaging system. Unlike the IPSF of a conventional imaging system, the IPSF of a catadioptric one with a curved mirror is spatially varying. To determine the suitability of focal sweep for extended DOF (EDOF) catadioptric imaging, we seek to address the following questions: (a) For any given point in the image, what is the IPSF produced by a pre-selected focal sweep range? (b) How much scene information is preserved by this IPSF and how depth-invariant is it? (c) How does the IPSF vary over the space of the image? (d) What is the optimal sweep range for a desired DOF?

We begin by developing a ray-tracing system for computing the PSF of a catadioptric imaging system with given optical parameters. We use our ray-tracer to compute the

*He was a visiting scientist from Sony Corporation, Japan.

IPSF as a function of both image coordinates and focal sweep range. Next, we provide metrics for evaluating the sharpness of an IPSF and for determining how depth-invariant it is. These results indicate that for catadioptric system with curved mirrors, focal sweep can indeed be effective in extending DOF. We also develop a framework for deriving the optimal sweep range while taking field curvature and astigmatism into account.

We conducted several experiments to validate the practical feasibility of our approach. Using an SLR camera, a motorized linear stage, and an Arduino controller, we built a focal sweep camera that allows us to control the sweep range and the exposure time. Using this system, we have extended the DOF of catadioptric systems that use spherical and paraboloidal mirrors. We conclude the paper with a comparison between catadioptric images captured with and without focal sweep.

2. Related Work

2.1. Extended Depth of Field

Several methods have been proposed to extend the DOF of imaging systems [4, 7, 8, 9, 12]. One approach is to use a coded aperture [19, 26, 27, 30], where a specially designed aperture is used to capture high frequency components of the scene. An EDOF image is recovered by deconvolving the captured image with a depth-dependent PSF. In addition to requiring prior knowledge regarding the 3D structure of the scene, this approach suffers from lower light efficiency as any coded aperture acts like a partial attenuator.

Focal sweep is another way to extend DOF [2, 6, 10, 17, 18]. Nagahara *et al*. [20] used a camera that translates the image sensor during the exposure time of the sensor. They showed that the IPSF of their focal sweep camera is nearly space-invariant and depth-invariant. An EDOF image is computed by deconvolving the captured image with the IPSF. In contrast to all of the above work, our goal is to investigate the viability of focal sweep for extending the DOF of catadioptric imaging systems.

The simplest way to achieve EDOF is to simply stop down the aperture. However, Cossairt *et al*. [5] found that computational imaging methods that use optical coding and decoding such as focal sweep achieve better performance (in terms of SNR) than stopped-down apertures at low light levels (e.g., lower than 125 lux). Moreover, a stopped-down aperture lowers image quality due to diffraction. In Sec. 5, we demonstrate the advantage of using focal sweep over a stopped-down aperture at low light levels.

2.2. Catadioptric Imaging Systems

Catadioptric imaging systems with curved mirrors suffer from two types of optical aberrations that arise due to the mirrors' curvature and the finite lens aperture: (a) field curvature, which causes space-varying blur over the extent of the mirror; and (b) astigmatism, which forms two separated focal images for a pencil of light rays emitted from a single point. A detailed analysis by Baker and Nayar [1] describes the properties of the blurring caused by a curved mirror. The first aberration, field curvature, is a common optical problem, where the curvature of the mirror causes the focal surface to be curved. Fig. 1 illustrates the effect of the second aberration, astigmatism. Assuming the mirror is rotationally symmetric, the plane containing both the chief ray (which is the light ray passing through the center of a camera's aperture) and the mirror's axis of rotation is called the meridional plane (or tangential plane), and the plane containing the chief ray which is perpendicular to the meridional plane is called sagittal plane [11]. As Fig. 1 shows, an oblique pencil of light rays emitted from a world point produces two separated focal images: the meridional and the sagittal images. Now consider all world points within the FOV of the imaging system that are at the same distance from the mirror surface. The envelopes of the meridional and sagittal focal images produced by this entire set of world points are referred to as the meridional and sagittal focal surfaces, respectively.

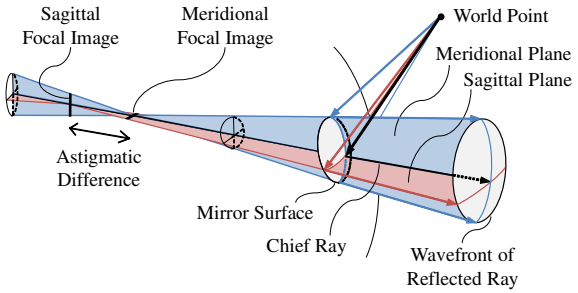

Figure 1: Astigmatism caused by a reflective mirror. A pencil of light rays that is emitted from a world point and reflected on a curved mirror produces two line-shaped virtual images, which are mutually-perpendicular, at different positions provided the incident direction of a chief ray is oblique to the mirror's axis of rotation.

Swaminathan [24] used caustics to model the meridional focal image produced by catadioptric imaging systems. He found that an infinite range of scene depths produces meridional focal images that are contained within a finite volume called the caustic volume. However, the sagittal focal image was not considered in his study. Based on the caustic volume, Li and Li [16] developed a method to extend the DOF of catadioptric imaging systems by capturing a focal stack (a set of images corresponding to different focus settings) and then combining the best-focused annuli from the images in the stack. Although they addressed the problem of field curvature, they did not consider astigmatism. Kuthirummal [14] deblurred images captured by a catadioptric imaging system with spatially varying PSFs to extend DOF, but this approach cannot fully recover frequencies that

are lost due to strong blurring in some image regions.

In this paper, we overcome the effects of both field curvature and astigmatism by using a single image captured during focal sweep. As the focal plane is swept across the curved mirror, the high frequency content corresponding to each region on the mirror is guaranteed to be captured during the sweep. We also develop a method for deriving the optimal focal sweep range by analyzing the locations of both the meridional and sagittal focal surfaces.

3. Analysis of PSFs of Catadioptric Cameras

An EDOF image is obtained by deconvolving the captured focal sweep image with an IPSF, which can vary significantly over the surface of the mirror. In this section, we analyze the IPSF for a spherical and a paraboloidal mirror by using ray tracing to confirm that the IPSF produced at each location on the mirror is quasi depth-invariant and hence useful for EDOF. A metric is provided to evaluate the quality (sharpness and depth-invariance) of the IPSF.

3.1. PSFs for a Curved Mirror

Fig. 2 illustrates the imaging model we have used for our analysis. A camera is placed above a rotationally symmetric curved mirror. The lens is assumed to obey the thin lens equation:

$$\frac{1}{f} = \frac{1}{i} + \frac{1}{o}, \tag{1}$$

where f is the focal length of the lens, i is distance between the lens and the image plane, and o is distance between the lens and the focal plane.

Fig. 3 shows the simulated PSFs for a spherical mirror captured by the camera. The diameter of the mirror is 50 mm and its center is placed 352 mm from the lens. Several world points (point light sources) are placed 50 cm from each reflecting point. The focal length of the lens is 50 mm and F-number is 2.8. When the image sensor is translated in the vertical direction, the focal plane also moves in the vertical direction, and the size and shape of the image blur varies. Due to astigmatism, none of the image points (except the one that lies at the center of the mirror) is perfectly focused for any position of the image sensor. The PSFs in the periphery of the mirror change significantly in the tangential and the radial directions because of the gap between the meridional and sagittal focal images. The line-shaped PSFs shown in the red frames in Figs. 3b and 3d correspond to the meridional and the sagittal focal images, respectively. Note that these images are severely blurred along one direction, whereas high frequency content along the perpendicular direction is preserved.

Fig. 4a shows the IPSFs of this spherical setup. We obtained them by adding the PSFs for 26 focal planes between 339 mm and 364 mm. The second column shows magnified IPSFs calculated for world points placed 50 cm from

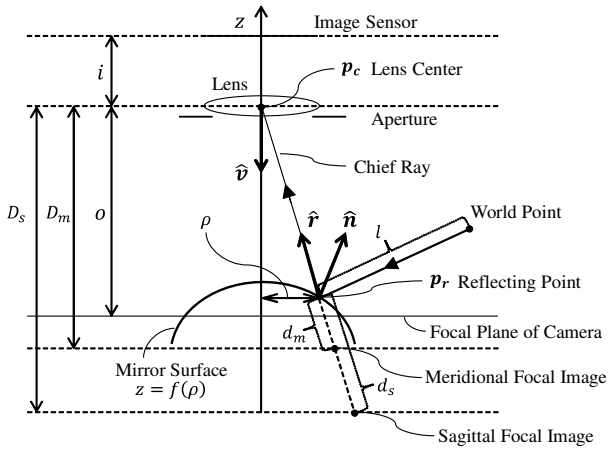

Figure 2: Cross-section of imaging model along meridional plane. A camera is placed above a rotationally symmetric mirror. The optical axis of the camera is assumed to be coincident with the mirror's axis of rotation. A light ray emitted from a world point is reflected at a point $\boldsymbol{p_r}$ on the mirror surface. The distance between the world point and $\boldsymbol{p_r}$ is l. The reflected ray is captured by the camera after passing through the lens center located at $\boldsymbol{p_c}$. Meridional and sagittal focal images are produced at distance of d_m and d_s from the reflecting point along the reflection direction, respectively. A vector $\hat{\boldsymbol{n}}$ is a unit normal vector of the mirror at the reflecting point, $\hat{\boldsymbol{r}}$ is a unit vector of reflection direction, and $\hat{\boldsymbol{v}}$ is a unit vector of the camera's viewing direction.

the mirror surface, and the plots on the right show cross-sections of IPSFs for the same mirror locations but different world point distances. The shapes of the IPSFs are spatially varying, as seen in Fig. 4a. Fig. 4a also shows that the shapes of the IPSFs corresponding to the same mirror location but different depths are almost depth-invariant (quasi depth-invariant), which suggests that they can be used for deconvolution of the focal sweep image to achieve EDOF. Note that the shape of the IPSF is determined only by the radial distance of the image point from the center—the IPSF simply rotates in the tangential direction.

In another simulation, the vertex of a paraboloidal mirror with diameter of 56.5 mm, focal length of 14.1 mm and height of 14.1 mm, is placed 352 mm from the lens. Fig. 4b shows IPSFs for this setup, which is obtained by adding the PSFs for 22 focal planes between 366 mm and 387 mm. Fig. 4c shows IPSFs for the paraboloidal mirror tilted around its vertex at an angle of 30°, which is obtained by adding the PSFs for 27 focal planes between 363 mm and 389 mm. The IPSFs are quasi depth-invariant in the case of the paraboloidal mirror and the tilted one as well. For the on-axis paraboloidal mirror, the IPSFs do not vary across the mirror surface as much as in the spherical and tilted paraboloidal cases because the astigmatism is lower. While the IPSF is almost always cross-shaped (irrespective

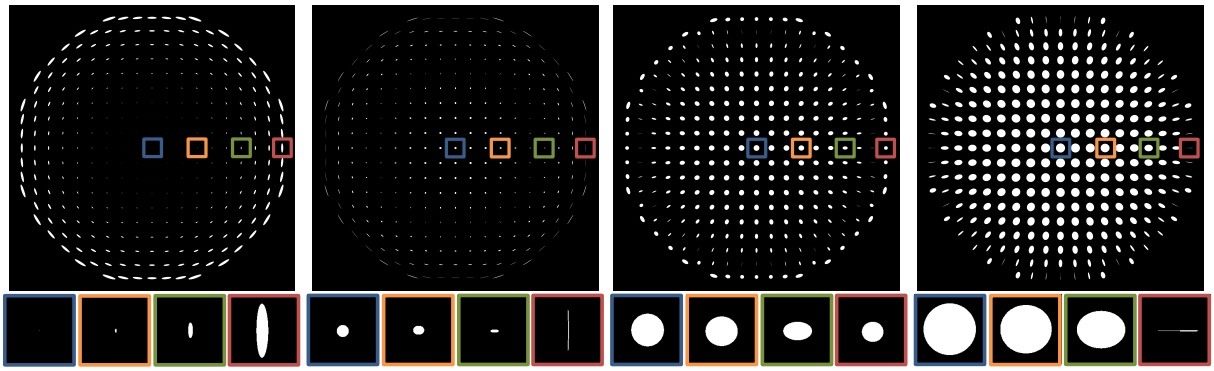

(a) Focused at 339 mm. (b) Focused at 346 mm. (c) Focused at 359 mm. (d) Focused at 372 mm.

Figure 3: PSF for spherical mirror for different focal plane distances. The center of a spherical mirror of diameter 50 mm is placed 352 mm from the lens. Note that there is no focal plane position for which all points on the mirror are in focus. The peripheral part of the mirror has particularly strong blur. The PSF is squashed along the radial direction in (b), while it is squashed along the tangential direction in (d).

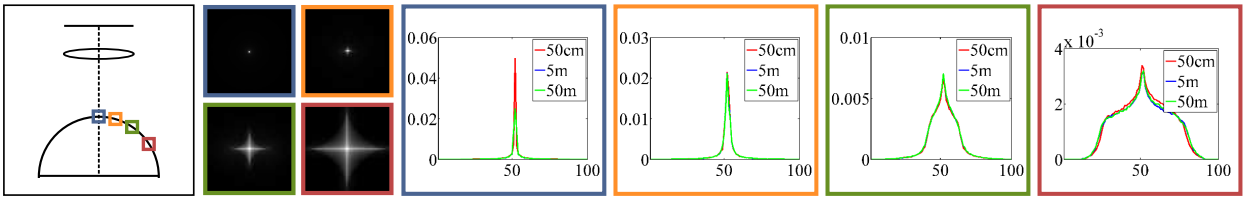

(a) IPSFs for spherical mirror.

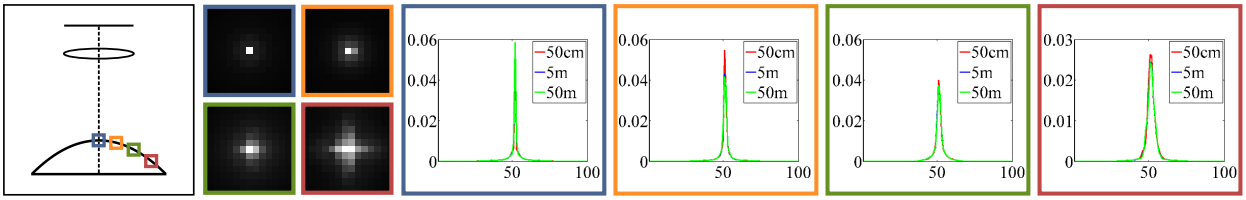

(b) IPSFs for paraboloidal mirror.

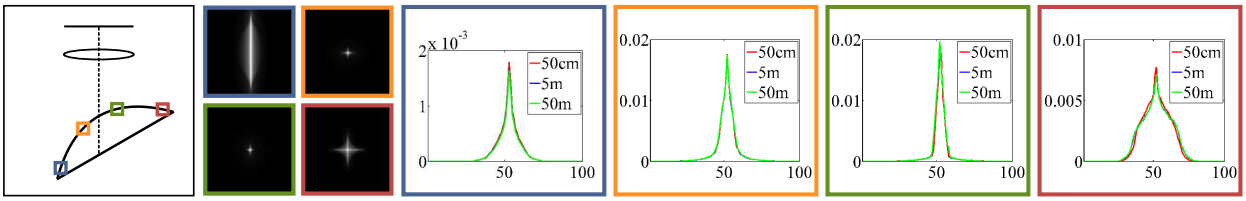

(c) IPSFs for tilted paraboloidal mirror.

Figure 4: The first column shows the relative positions of the image sensor, the lens and the mirror. The second column shows magnified IPSFs calculated for world points placed 50 cm from the mirror surface. The magnifications are different for each mirror and each IPSF is normalized by its maximum value for display purposes. The plots on the right are cross-sections of IPSFs along the radial direction of the mirror for the same mirror locations but different world point distances of 50 cm, 5 m and 50 m. Each IPSF is normalized by its area.

of the mirror shape and tilt), the one shown in the blue frame in Fig. 4c is large in the tangential direction. This indicates that in this region of the image the acquired focal sweep image will not capture high frequency content along the tangential direction unless the focal sweep range is enlarged.

3.2. Characteristics of IPSF and the Sweep Range

We now explore the relationship between the structure of the IPSF and the sweep range. Fig. 5 illustrates cross-sections of the IPSF for different sweep ranges and scene depths when a spherical mirror is placed at the same position as in Sec. 3.1. The sharper the IPSF, the more high frequency components it preserves, whereas an IPSF with low sharpness will produce image artifacts when it is used for deconvolution. As the sweep range increases, the sharpness of the IPSF at the center of the mirror decreases slightly, while the sharpness in the tangential direction for points in the periphery increases, and the peak value of the cross-

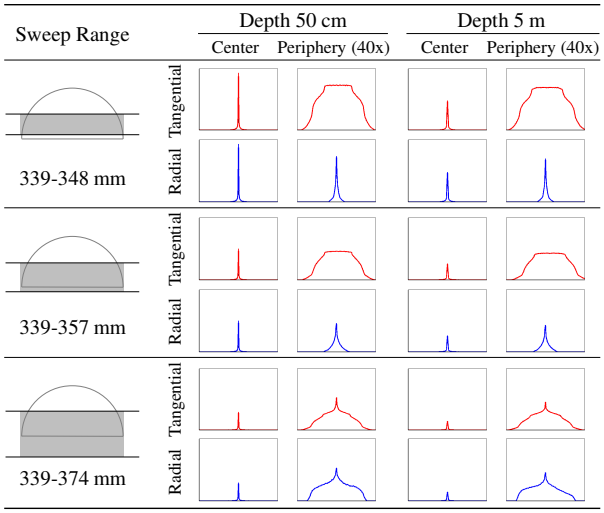

Figure 5: Cross-sections of IPSFs for spherical mirror for different sweep ranges and scene depths. The sweep range represents the distance swept by the focal plane, where the distance is measured from the lens. The IPSFs shown in red and blue correspond to tangential and radial directions in the image, respectively. The left plot of each column shows the IPSF at the center of the mirror, and the right plot shows the IPSF in the periphery. The vertical axis for the peripheral IPSF is scaled by 40. In all the simulations, the same exposure time is assumed.

Sweep Range [mm]	IPSF Depth Variance	IPSF Sharpness (Kurtosis)			
		Image Center		Image Periphery	
		Tangential	Radial	Tangential	Radial
$339-348$	3.2×10^2	117.5	117.5	1.28	50.6
$339-357$	4.6×10^2	116.4	116.4	1.34	21.8
$339-374$	1.6×10^2	115.9	115.9	1.99	2.12

Table 1: IPSF variance due to depth measured using L2 norm of the Wiener reconstruction error and sharpness of IPSF measured using kurtosis.

section along the radial direction in the periphery remains approximately constant. This result demonstrates that by using a large sweep range, it is possible to achieve EDOF over a large FOV. We also note that shape of each IPSF is approximately depth-invariant.

We verify some of the above observations using quantitative metrics. The sharpness of the IPSF can be quantified using kurtosis, which is a measure of the sharpness of any given distribution. The kurtosis has a value of 3 for the standard normal distribution, with values greater than 3 indicating higher sharpness. The average kurtoses of the IPSF cross-sections over depths of 50 cm, 1 m, 5 m, and 10 m are shown in Table 1. The sharpness in the tangential direction for the periphery increases as the sweep range increases. At the same time, the sharpness along both directions at the center of the mirror and that of the radial direction for the periphery decreases. This effect captured a trade-off inherent to focal sweep—to increase image quality in the periphery, image quality in the center must be sacrificed.

The variation of the IPSF over a depth range (IPSF variance due to depth) can be quantified using the distance between the IPSFs. We use the L2 norm of the Wiener reconstruction error when an image is blurred with one IPSF and deconvolved with another. The following metric was introduced by Kuthirummal *et al*. [15]:

$$V\big(p_1(x,y),p_2(x,y)\big)=\sum_{u,v}\left(\frac{\big|P_1(u,v)-P_2(u,v)\big|^2}{\big|P_1(u,v)\big|^2+\epsilon}+\frac{\big|P_1(u,v)-P_2(u,v)\big|^2}{\big|P_2(u,v)\big|^2+\epsilon}\right)\big|W(u,v)\big|^2, \tag{2}$$

where $P_n(u,v)$ is the Fourier transform of the IPSF $p_n(x,y)$, $W(u,v)$ is a weighting term that accounts for the power fall-off for natural images, and ϵ is a small positive constant to ensure that the denominators are not zero. IPSFs at 19 equally-spaced locations along the radius of the mirror are simulated. The average of the IPSF variance due to depth for each sweep range is computed:

$$V_{avg}=\frac{1}{4}\sum_{j=1}^{4}\frac{1}{19}\sum_{k=1}^{19}V\big(p_{j,k}(x,y),p_{1,k}(x,y)\big), \tag{3}$$

where $p_{j,k}(x,y)$ is the IPSF for depth $\{d_j\}$=$\{$50 cm, 1 m, 5 m, 10 m$\}$ and location $\{l_k\}$ on the mirror. The computed values are shown in Table 1. Kuthirummal *et al*. [15] have shown that for a conventional imaging system (not using a curved mirror) the value of V in Eq. (2) for a range of scene depths that is similar to our case is of the order of 1.0×10^4. In comparison the values of V_{avg} (Eq. 3) shown in Table 1 are small, implying that our IPSFs are quasi depth-invariant.

4. Optimal Focal Sweep Range

The optimal sweep range is derived so as to preserve high frequency components within the desired DOF by sweeping the focal plane through both the meridional and sagittal focal surfaces. In this section, we derive the positions of the two focal surfaces formed by a curved mirror and develop a framework for deriving the optimal sweep range.

The Coddington equations [13], which calculate the positions of the meridional and the sagittal focal images for a spherical refractive surface, are well-known in the optics community. Burkhard and Shealy [3] used differential geometry to generalize these equations so that they can be applied to both refractive and reflective surfaces of arbitrary shape. Consider a rotationally symmetric mirror which is obtained by rotating a curve $z=f(\rho)$ around the z axis, where ρ denotes the radial distance from any point on the mirror surface to the z axis. Note that the range of ρ determines the FOV of the catadioptric imaging system. Once again, consider Fig. 2. If the chief ray lies on the meridional

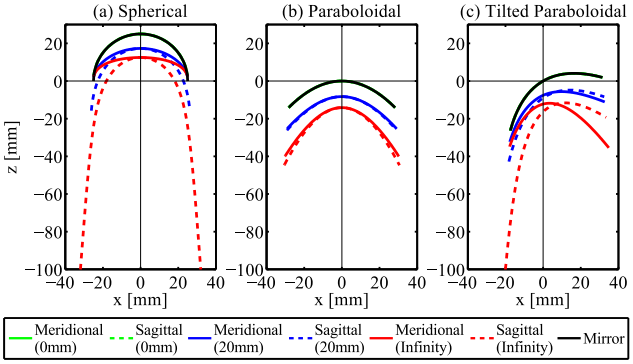

Figure 6: Meridional and sagittal focal surfaces for different scene depths: 0 mm, 20 mm, and infinity. The green-colored lines, which denote the focal surfaces for scene depth 0 mm, are located exactly on each mirror surface.

plane, the generalized Coddington equations are:

$$d_m = (lR_m\hat{\boldsymbol{n}}\cdot\hat{\boldsymbol{r}})/(2l + R_m\hat{\boldsymbol{n}}\cdot\hat{\boldsymbol{r}}),$$
$$R_m = \left[1+\left(f'(\rho)\right)^2\right]^{\frac{3}{2}}/f''(\rho), \tag{4}$$

$$d_s = lR_s/(2l\hat{\boldsymbol{n}}\cdot\hat{\boldsymbol{r}} + R_s),$$
$$R_s = \rho\left[1+\left(f'(\rho)\right)^2\right]^{\frac{1}{2}}/f'(\rho), \tag{5}$$

where, d_m is distance from the reflecting point to the meridional focal image, R_m is the principal radius of curvature of the reflecting surface for the meridional plane, d_s is distance from the reflecting point to the sagittal focal image, R_s is the principal radius of curvature of the reflecting surface for the sagittal plane, and l is distance between the world point and the reflecting point. Taking the limit $l \to \infty$ in Eq. (4) yields $d_m = (R_m\hat{\boldsymbol{n}}\cdot\hat{\boldsymbol{r}})/2$, which forms a surface equivalent to the boundary of the caustic volume derived by Swaminathan [24]. Fig. 6 illustrates the cross-sections of the meridional and sagittal focal surfaces along the meridional plane for different scene depths. The shapes and the positions of the mirrors are identical to those used in Sec. 3.

The distances from the lens to the meridional and sagittal focal images along the camera's optical axis are given by:

$$D_m(\rho, l) = \left|(\boldsymbol{p_r} - d_m\hat{\boldsymbol{r}} - \boldsymbol{p_c})\cdot\hat{\boldsymbol{v}}\right|, \tag{6}$$
$$D_s(\rho, l) = \left|(\boldsymbol{p_r} - d_s\hat{\boldsymbol{r}} - \boldsymbol{p_c})\cdot\hat{\boldsymbol{v}}\right|. \tag{7}$$

The optimal sweep range $[D^{opt}_{\min}, D^{opt}_{\max}]$ for desired range of ρ and l is determined as:

$$D^{opt}_{\min} = \min_{\rho\in P, l\in L}\left\{D_m(\rho,l), D_s(\rho,l)\right\}, \tag{8}$$
$$D^{opt}_{\max} = \max_{\rho\in P, l\in L}\left\{D_m(\rho,l), D_s(\rho,l)\right\}, \tag{9}$$

where $P = [\rho_{\min}, \rho_{\max}]$ and $L = [l_{\min}, l_{\max}]$. In this paper, $\rho_{\min}$ is assumed to be zero. Once P (i.e., FOV) and L (i.e., depth range) are provided, the optimal sweep range is determined using Eqs. (4)–(9). Note that this framework can be extended to any catadioptric imaging system (consisting of a mirror with an arbitrary shape) by using Burkhard and Shealy's method [3] instead of Eqs. (4) and (5).

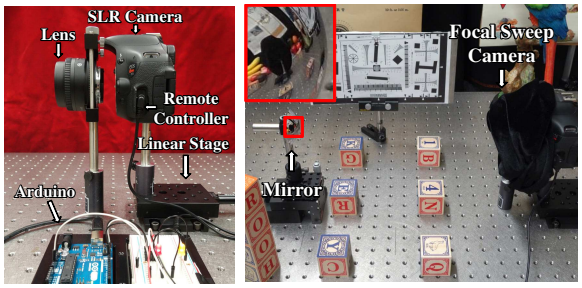

(a) Focal sweep camera. (b) Experimental setup.

Figure 7: A conventional SLR camera body is combined with a motorized linear stage as shown in (a), which enables it to sweep the focal plane by translating the image sensor. (b) Experimental setup. The curved mirror is put in front of the focal sweep camera.

5. Experiments

In this section, we show several experiments to demonstrate the practical feasibility of our framework. Our catadioptric systems use spherical and paraboloidal mirrors. As a result, we obtain EDOF images by deconvolving the focal sweep images with pre-computed IPSFs.

5.1. Focal Sweep System with Curved Mirrors

The hardware setup for our focal sweep camera is shown in Fig. 7. It uses an SLR camera body and a 50 mm, f/2.8 lens. The camera body can be translated with respect to the lens using a motorized linear stage. The velocity of the stage was set to 1 mm/sec in all our experiments. A shutter trigger is generated by a remote controller which is connected to an Arduino controller. The Arduino and the linear stage are connected to a PC to synchronize image exposure and camera translation. The shapes and the positions of the mirrors are identical with those used for our analysis in Sec. 3. The distances of scene objects from the mirror range from about 10 cm to about 3 m.

Fig. 8 illustrates the processing pipeline for obtaining an EDOF image. (a) First, we pre-compute IPSFs for scene depth of 50 cm for 19 equally-spaced locations along the radius of the mirror. (b) The IPSFs image is converted from Cartesian to polar coordinates. (c) The focal sweep image captured with our camera is converted from Cartesian to polar coordinates. (d) Then, we deconvolve the captured image (using Wiener filtering) with a single cropped IPSF for each line since the shapes of the IPSFs for any given radial distance from the center of the mirror are exactly the same in Cartesian coordinates. (e) Finally, The deconvolved image is converted back from polar to Cartesian coordinates. In the tilted paraboloidal case, where the optical axis of the camera is not coincident with the mirror's axis of rotation, we compute 970 spatially varying IPSFs for the entire sur-

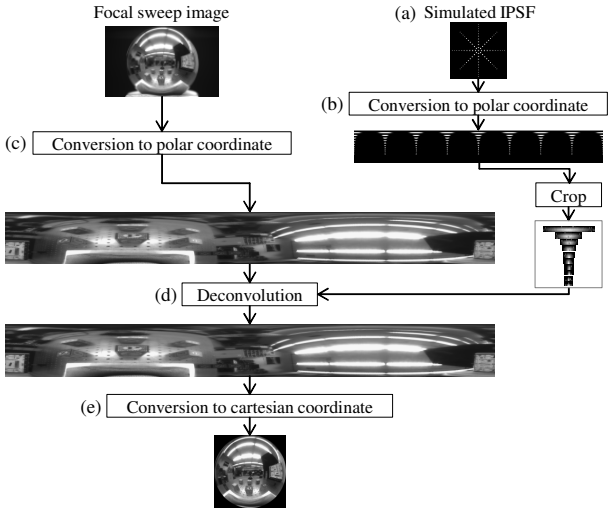

Figure 8: Processing pipeline.

face of the mirror, then use them to deconvolve the focal sweep image in Cartesian coordinates. The same IPSF is used in each small image region assuming that the blurs are nearly invariant in each region.

5.2. EDOF Images of Curved Mirrors

For the spherical mirror, for an FOV of 237°and depth range of 30 cm–10 m, the optimal sweep range was found to be 339–364 mm using Eqs. (4)–(9). The corresponding translation distance of the image sensor is 0.69 mm, which is determined using Eq. (1). An example EDOF image is shown in Fig. 9b. As Fig. 9a shows, the image captured with a normal camera has a lot of blurring, especially in the periphery. Straight lines along the radial direction are strongly blurred, and only the straight lines along the tangential direction are more or less preserved because they are principally blurred along the tangential direction (see Fig. 3a). In contrast, Fig. 9b shows that the peripheral region in the EDOF image retains high frequency components in both the radial and the tangential directions. Hence, sweeping the focal plane across the meridional and the sagittal focal surfaces enables the deconvolution to preserve the high frequency components in both directions.

For the paraboloidal mirror, for an FOV of 167°and depth range of 30 cm–10 m, the optimal sweep range was found to be 366–387 mm. The corresponding translation distance of the image sensor is 0.50 mm. An example EDOF image is shown in Fig. 9d. For the tilted paraboloidal mirror, for an FOV of 147°along the meridional plane and depth range of 30 cm–10 m, the optimal sweep range was found to be 363–389 mm. The corresponding translation distance of the image sensor is 0.60 mm. Fig. 9f shows the result, which proves the effectiveness of our method in a case where the optical axis of the camera and the mirror's axis of rotation are not coincident. The blurring caused by the on-axis paraboloidal mirror is reduced more

Figure 10: Comparison between EDOF image captured using our method (top row) and image captured with a normal camera using a stopped-down aperture (bottom row) for a scene brightness of about 50 lux. The former is captured with F2.8, 0.6 sec, and ISO100. The latter is captured with F11, 0.6 sec, and ISO1600.

than the blurring due to the spherical mirror and the tilted paraboloidal mirror (see Fig. 9) because the astigmatism is lower in this case (see Fig. 6). Note that, in all cases, the central regions of the EDOF images are blurred slightly more than the central region of the image captured with a normal camera: this is the inherent trade-off in using focal sweep, as described in Sec. 3.2.

Fig. 10 compares an image captured using focal sweep (using the paraboloidal mirror) with one captured using aperture-stopping for a dimly lit scene. The EDOF image using focal sweep has less noise than that using a stopped-down aperture because its light throughput is higher.

6. Conclusion

In this paper, we presented a novel framework for extending the DOF of catadioptric imaging systems consisting of curved mirrors by using focal sweep. Using a ray-tracer for computing IPSFs, we showed that while the IPSF is spatially varying when a curved mirror is used, it remains quasi depth-invariant over the wide FOV of the imaging system. We presented metrics for evaluating the quality (sharpness and depth-invariance) of the IPSF. We also developed a framework for finding the optimal sweep range by analyzing the locations of both the meridional and the sagittal focal surfaces, both of which are effected by field curvature and astigmatism. Using a prototype focal sweep camera, we conducted several experiments to demonstrate the practical feasibility of our approach. We showed EDOF images captured by spherical and paraboloidal (both on-axis and off-axis) catadioptric systems. Focal sweep enabled the system to preserve high frequency information over the entire FOV.

Our results are applicable to any given catadioptric imaging system. Once the mirror shape, camera parameters, desired FOV and depth range are specified, our framework can be used to evaluate the IPSF of the system and determine the optimal focal sweep range. From a broader perspective, our results can be used to reduce the optical complexity of catadioptric imaging systems.

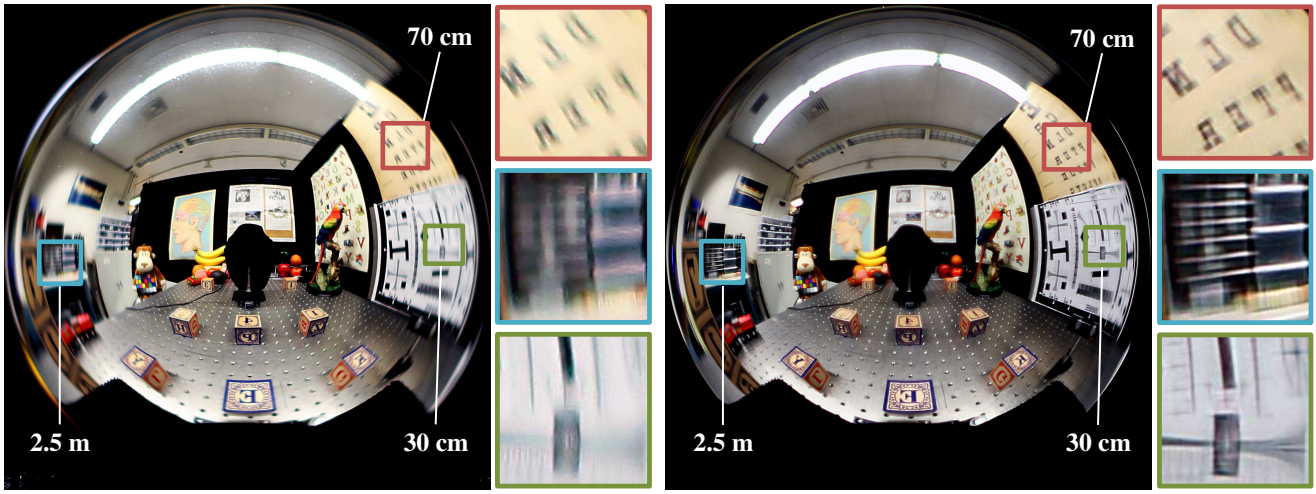

(a) Spherical mirror: Conventional.

(b) Spherical mirror: Focal sweep (EDOF).

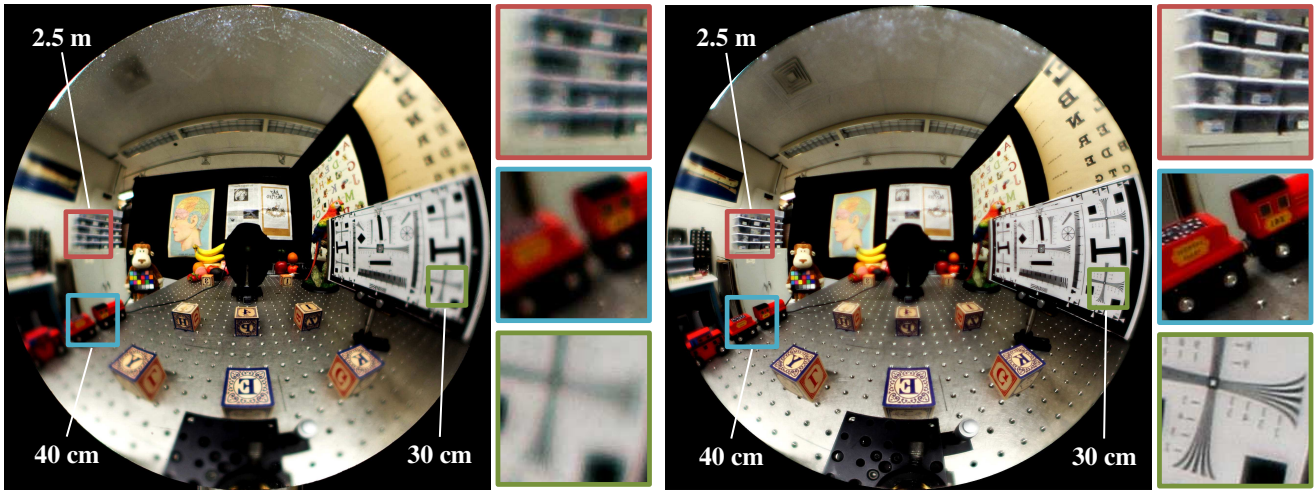

(c) Paraboloidal mirror: Conventional.

(d) Paraboloidal mirror: Focal sweep (EDOF).

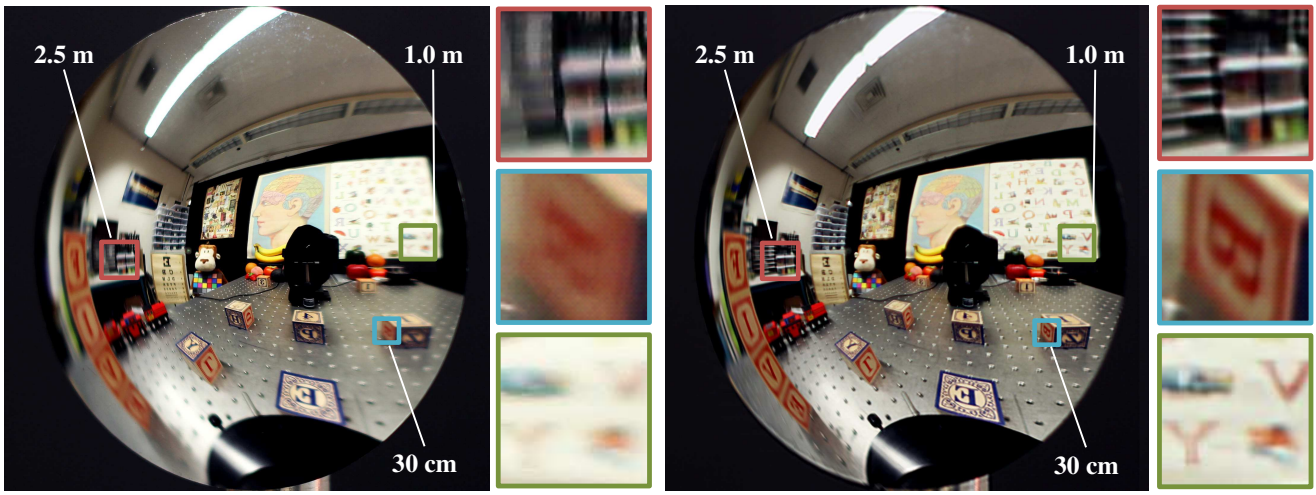

(e) Tilted paraboloidal mirror: Conventional.

(f) Tilted paraboloidal mirror: Focal sweep (EDOF).

Figure 9: The left column shows images captured with a normal camera by focusing at the center of the mirror. The right column shows EDOF images computed by deconvolving focal sweep images captured using our camera with the pre-computed IPSFs. The approximate distances of the magnified regions from the mirror surface are noted in each image.

References

[1] S. Baker and S. K. Nayar. A theory of single-viewpoint catadioptric image formation. *International Journal on Computer Vision*, 35(2):175–196, 1999.

[2] Y. Bando, H. Holtzman, and R. Raskar. Near-invariant blur for depth and 2D motion via time-varying light field analysis. *ACM Transactions on Graphics*, 32(2):13:1–13:15, 2013.

[3] D. G. Burkhard and D. L. Shealy. Simplified formula for the illuminance in an optical system. *Applied Optics*, 20(5):897–909, 1981.

[4] A. Castro and J. Ojeda-Castaneda. Asymmetric phase masks for extended depth of field. *Applied Optics*, 43(17):3474–3479, 2004.

[5] O. Cossairt, M. Gupta, and S. K. Nayar. When does computational imaging improve performance? *IEEE Transactions on Image Processing*, 22(2):447–458, 2013.

[6] O. Cossairt and S. K. Nayar. Spectral focal sweep: Extended depth of field from chromatic aberrations. In *IEEE International Conference on Computational Photography*, pages 1–8, 2010.

[7] O. Cossairt, C. Zhou, and S. K. Nayar. Diffusion coded photography for extended depth of field. *ACM Transactions on Graphics*, 29(4):31:1–31:10, 2010.

[8] E. Dowski and W. Cathey. Extended depth of field through wave-front coding. *Applied Optics*, 34(11):1859–1866, 1995.

[9] N. George and W. Chi. Extended depth of field using a logarithmic asphere. *Journal of Optics A: Pure and Applied Optics*, pages 157–163, 2003.

[10] G. Hausler. A method to increase the depth of focus by two step image processing. *Optics Communications*, 6(1):38–42, 1972.

[11] E. Hecht. *Optics*. Addison-Wesley, fourth edition, 1998.

[12] G. Indebetouw and H. Bai. Imaging with Fresnel zone pupil masks: extended depth of field. *Applied Optics*, 23(23):4299–4302, 1984.

[13] R. Kingslake. Who discovered Coddington's equations? *Optics and Photonics News*, 5(8):20–23, 1994.

[14] S. Kuthirummal. *Flexible imaging for capturing depth and controlling field of view and depth of field*. PhD thesis, Columbia University, New York, 2009.

[15] S. Kuthirummal, H. Nagahara, C. Zhou, and S. K. Nayar. Flexible depth of field photography. *IEEE Transactions on Pattern Analysis and Machine Intelligence*, 33(1):58–71, 2011.

[16] W. Li and Y. Li. Overall well-focused catadioptric image acquisition with multifocal images: A model-based method. *IEEE Transactions on Image Processing*, 21(8):3697–3706, 2012.

[17] S. Liu and H. Hua. Extended depth-of-field microscopic imaging with a variable focus microscope objective. *Optics Express*, 19(1):353–362, 2011.

[18] D. Miau, O. Cossairt, and S. K. Nayar. Focal sweep videography with deformable optics. In *IEEE International Conference on Computational Photography*, pages 1–8, 2013.

[19] M. Mino and Y. Okano. Improvement in the OTF of a defocused optical system through the use of shaded apertures. *Applied Optics*, 10(10):2219–2225, 1971.

[20] H. Nagahara, S. Kuthirummal, C. Zhou, and S. K. Nayar. Flexible depth of field photography. In *European Conference on Computer Vision*, pages 60–73, 2008.

[21] S. K. Nayar. Sphereo: Determining depth using two specular spheres and a single camera. In *SPIE Conference on Optics, Illumination, and Image Sensing for Machine Vision III*, pages 245–254, 1988.

[22] S. K. Nayar. Catadioptric omnidirectional camera. In *IEEE Conference on Computer Vision and Pattern Recognition*, pages 482–488, 1997.

[23] D. W. Rees. Panoramic television viewing system. United States Patent No. 3,505,465, 1970.

[24] R. Swaminathan. Focus in catadioptric imaging systems. In *IEEE International Conference on Computer Vision*, pages 1–7, 2007.

[25] S. Trubko, V. N. Peri, S. K. Nayar, and J. Korein. Super wide-angle panoramic imaging apparatus. United States Patent No. 6,611,282, 2003.

[26] A. Veeraraghavan, R. Raskar, A. Agrawal, A. Mohan, and J. Tumblin. Dappled photography: Mask enhanced cameras for heterodyned light fields and coded aperture refocusing. *ACM Transactions on Graphics*, 26(3), 2007.

[27] W. Welford. Use of annular apertures to increase focal depth. *Journal of the Optical Society of America*, 50(8):749–753, 1960.

[28] Y. Yagi and S. Kawato. Panoramic scene analysis with conic projection. In *IEEE/RSJ International Conference on Robots and Systems*, pages 181–187, 1990.

[29] J. Y. Zheng and S. Tsuji. Panoramic representation for route recognition by a mobile robot. *International Journal of Computer Vision*, 9(1):55–76, 1992.

[30] C. Zhou and S. K. Nayar. What are good apertures for defocus deblurring? In *IEEE International Conference on Computational Photography*, pages 1–8, 2009.